Scripta Materialia 222 (2023) 115055

Contents lists available at ScienceDirect

Scripta Materialia

journal homepage: www.journals.elsevier.com/scripta-materialia

Observations of unexpected grain boundary migration in $SrTiO_3$

Vivekanand Muralikrishnan [a], He Liu [b], Lin Yang [a], Bryan Conry [a], Christopher J. Marvel [c,2], Martin P. Harmer [c], Gregory S. Rohrer [b,3], Michael R. Tonks [a], Robert M. Suter [b], Carl E. Krill III [d], Amanda R. Krause [a,1,*]

[a] University of Florida, Gainesville, FL, USA
[b] Carnegie Mellon University, Pittsburgh, PA, USA
[c] Lehigh University, Bethlehem, PA, USA
[d] Ulm University, Ulm, Germany

ARTICLE INFO

Keywords:
High energy x-ray diffraction microscopy
Grain growth
Perovskite
Microstructure

ABSTRACT

High-energy x-ray diffraction microscopy (HEDM) nondestructively maps microstructures in 3D, allowing for the same grains and boundaries to be tracked over time during annealing experiments. Here, HEDM was applied to observe grain growth in strontium titanate. These results are compared to a 3D isotropic grain growth simulation that starts from the same initial microstructure to identify potentially unknown grain boundary migration mechanisms. During the simulation, grain growth behaves as expected: the change in grain volume is correlated with the number of neighbors, and the grain boundary velocity is correlated with its local curvature. Experimentally, however, flat boundaries were found to move faster than curved boundaries, and 37% of all measured boundaries move in the direction opposite to their curvature. These unexpected observations suggest that, in materials with anisotropic grain boundary properties, mechanisms other than curvature-driven boundary migration play a role in the minimization of interfacial energy.

Grain boundary (GB) migration in polycrystals often deviates from ideal grain growth, leading to poor predictability of the final processed microstructures. Burke and Turnbull derived that ideal parabolic grain growth results from GBs moving towards their center of curvature [1]. In general, deviations from ideal grain growth are often attributed to porosity [2], secondary phases [3], solute segregation [4], recrystallization driving forces [5], and/or anisotropic GB energy and mobility [6,7]. With so many factors influencing GB motion, it remains unclear the extent to which curvature directly contributes to grain growth in polycrystals with anisotropic GB properties. Bi-crystal experiments performed by Shvindlerman and colleagues in aluminum demonstrate that isolated GBs migrate at a rate proportional to their curvature and that the rate is dependent on misorientation [8]. However, these bi-crystal experiments remove any effects of neighboring GBs that may have competing driving forces for migration.

Recent developments of nondestructive, diffraction-based 3D x-ray microscopy (3D-XRM) methods provide an opportunity to directly investigate the role of curvature on grain growth in anisotropic polycrystals. Briefly, this method collects transmission x-ray diffraction patterns while a sample is rotating to reconstruct the location, size, orientation, and shape of each grain comprising the microstructure [9–13]. The non-destructive nature allows tracking of individual GBs and their neighborhoods at different stages of grain growth to produce a 4D (3D space + time) dataset.

Recent 3D-XRM studies reveal that polycrystalline grain growth can deviate from proposed theories. Patterson et al. investigated the role of curvature and number of neighbors on grain growth in Armco iron [14]. They found that, on average, the change in grain volume with time is proportional to the curvature of the individual grain. However, significant variation was observed, suggesting local fluctuations in GB motion. The local phenomenon was explored by Bhattacharya et al. in commercially-pure Ni [15]. Surprisingly, they did not observe any clear

* Corresponding author.
E-mail address: krause@cmu.edu (A.R. Krause).
[1] Present address: Carnegie Mellon University, Pittsburgh, PA, USA.
[2] Present address: Louisiana State University, Baton Rouge, LA, USA.
[3] Greg Rohrer was an Editor of the journal during the review period of the article. To avoid a conflict of interest, Greg Rohrer was blinded to the record and another editor processed this manuscript.

https://doi.org/10.1016/j.scriptamat.2022.115055
Received 15 July 2022; Received in revised form 13 September 2022; Accepted 14 September 2022

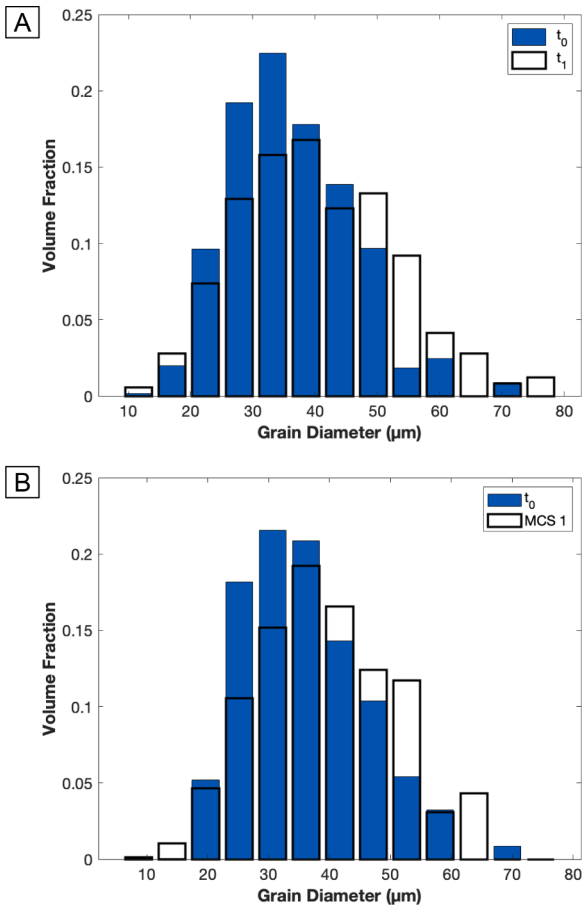

Fig. 1. Grain size distributions for the matched grains in the (A) HEDM scans and (B) SPPARKS simulations before and after growth.

trend between curvature and velocity for individual GBs. Instead, they found that the velocity could be correlated to the macroscopic GB character, independently of curvature, when considering all five degrees of freedom. It is unclear if this observation is unique to Ni or reflects a general trend in real polycrystals.

The purpose of this communication is to explore the role of curvature on GB migration in $SrTiO_3$, a model ceramic that contains no residual stress or other known driving forces besides interfacial energy, using high energy x-ray diffraction microscopy (HEDM; a type of 3D-XRM). The HEDM results are compared to those of a 3D isotropic grain growth model that starts from the same microstructure as measured experimentally. The grain volume change as a function of the number of nearest neighbors and the distance traversed by a GB as a function of its curvature are evaluated in both datasets.

The bulk $SrTiO_3$ sample was prepared by solid-state synthesis [16]. HEDM scans were collected after heat treating the $SrTiO_3$ monolith in forming gas at 1400 °C for 10 hr (t_0) and then an additional 70 hr (t_1). Samples were embedded in a Sr-rich sacrificial powder ($Sr_3Ti_2O_7$) to reduce the volatilization of SrO from the surface at 1400 °C [17]. The HEDM measurements were collected at the 1–ID beamline of the advanced photon source at Argonne National Laboratory [11]. The sample was mapped with 50 and 52 consecutive layers spaced 2 μm apart, totaling 100 μm and 104 μm, for the t_0 and t_1 scans, respectively. The HEDM data was reconstructed by converting the diffraction images to voxelated data using the HEXOMAP package [18]. Data clean-up and grain segmentation procedures were carried out on the reconstructed voxelated data using DREAM.3D [19]. Grain registration between scans was completed by identifying grains with center-of-mass distances less than 20 μm and misorientations below 1.5°. In this manner, 3196 of the

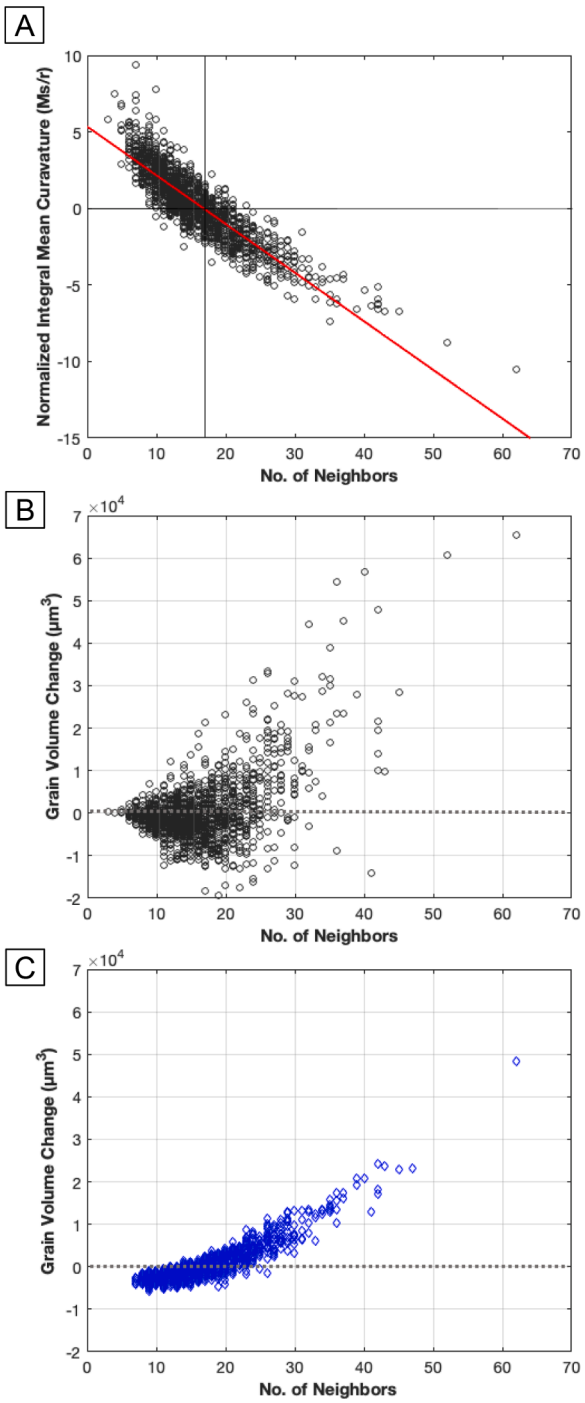

Fig. 2. Investigation of von Neumann-Mullins relationship in HEDM and SPPARKS. (A) Scatter plot of the grains' normalized integral mean curvatures according to their number of neighbors at t_0. The red line indicates the fitted trend line ($R^2 = 0.78$), which crosses the x-axis at 16.8 neighbors. The change in volume from t_0 to t_1 for each grain plotted according to its number of neighbors observed in the (B) HEDM scans and (C) SPPARKS simulation.

5463 and 3859 grains in the first and second scan, respectively, were registered. All grains and GBs that touch the sample surface or scan edges are excluded from this analysis. Additional details of sample synthesis and HEDM parameters are provided in the supplemental information.

The observed grain growth behavior was compared to a 3D isotropic Monte Carlo Potts simulation run via SPPARKS (Stochastic Parallel Particle Kinetic Simulator) [20], as described in the supplemental

material. Here, the initial condition for the SPPARKS simulation is the t_0 HEDM scan. The SPPARKS simulation was performed with a pseudo-temperature value that has been previously shown to produce grain size distributions that agree with theoretical predictions [21,22]. The microstructure was evolved from the t_0 condition until it reached 3570 grains, which is similar to the number of grains indexed in the t_1 HEDM scan.

Fig. 1A shows the grain size distribution for the t_0 and t_1 HEDM scans, excluding grains that could not be matched between datasets. The grain size distribution shows evidence of measurable grain growth. The mean equivalent spherical grain diameter increases from 21 μm to 24 μm (equivalent to a volume change of nearly 2400 μm^3) when considering both matched and unmatched grains but decreases (from 25 μm to 23 μm) if calculated with only matched grains. This difference is likely because the t_0 unmatched grain population includes many small grains that shrink to undetectable sizes and, thus, are not matched in the t_1 scan. Fig. 1B shows the grain size change observed in the SPPARKS simulation after growth, showing a similar evolution in grain size (increases from 21 μm to 23 μm) as the experimental observations.

First, we investigate the von Neumann [23] and Mullins [24] relation that predicts that the number of neighbors is correlated with curvature and, thus, grain growth. In an isotropic 2D system, a six-sided grain will not grow or shrink because its boundaries are flat to maintain equilibrium at the triple junctions and minimize interfacial energy. Grains with fewer than six sides will have convex boundaries and, thus, shrink, while grains with more than six sides will grow due to their concave boundaries. Although a tetrakaidecahedron (14-sided polygon) is the space-filling structure that meets the criteria for flat boundaries in 3D, previous experimental results have found that the curvature is zero for grains with 16 sides in $SrTiO_3$ [25]. Here, this value was verified by comparing each grain's normalized integral mean curvature with its number of sides, shown in Fig. 2A. Instead of determining the curvature from a smooth mesh that approximates the measured boundary position, the integral mean curvature (M_s) was determined from the voxels using the approach proposed by Patterson and colleagues [14,26]. M_s was calculated using the equation

$$M_s = \frac{\pi}{4} \times (N_{out} - N_{in}), \quad (1)$$

where N_{in} is the number of voxel edges formed by inward-angled concave voxel faces on the grain or GB of interest and N_{out} is the total number of edges formed by outward-angled convex voxel faces. This value is normalized by dividing it by the grain's radius (r).

Fig. 2A shows that Ms/r is correlated with the number of neighbors in the t_0 scan. Similar to previous 3D measurements of $SrTiO_3$ [25], the critical number of neighbors demarking when the curvature is zero is estimated to be 16.8 using the red fitted line ($R^2 = 0.78$) shown in Fig. 2A. However, Fig. 2B shows that the number of neighbors is not a good indicator of whether a grain will grow, shrink or maintain constant volume. Furthermore, no noticeable change in behavior is observed at ~17 neighbors; i.e., grains with as few as 7 neighbors grew and with as many as 41 neighbors shrank. In contrast, the isotropic simulation (Fig. 2C) followed the expected trend with greater fidelity. Furthermore, Fig. 2C shows that the critical number of faces that demarks shrinking and growing grains is ~17 (grains with as few as 12 neighbors grew and as many as 26 neighbors shrank), which agrees with the linear fit to the data of Fig. 2A. This suggests that the GBs in the simulation are generally moving according to curvature (i.e., the change in grain area is proportional to time), but not those in the experiment.

To test whether the discrepancy between simulation and experiment is due to local GB motion, a velocity term and GB curvatures were extracted from the 4D datasets. The GB motion is described by the metric GB distance traversed, which is defined as the volume traversed by the boundary during grain growth (dV) divided by the initial GB area (A). The dV for each individual GB is calculated as the net number of voxels that flip between neighboring grains, and A was calculated from the area

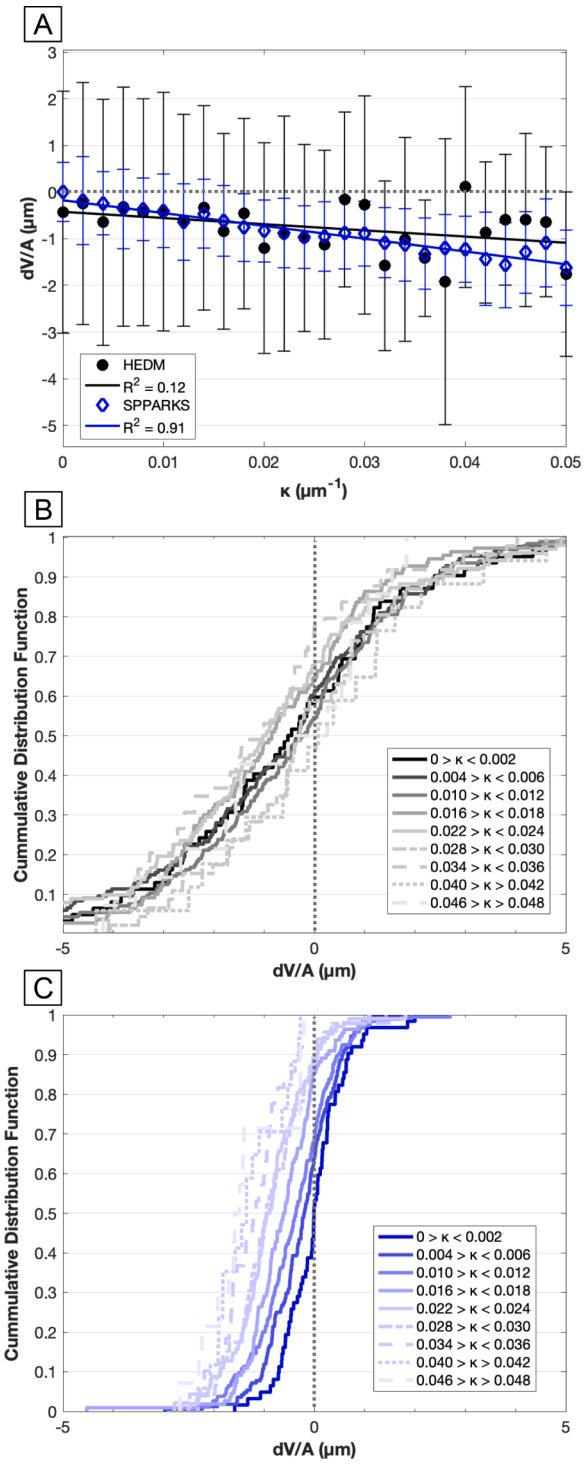

Fig. 3. (A) The average and standard deviation (error bars) of the distance traversed by a GB (dV/A) with respect to the boundary's mean curvature calculated from the HEDM scans and SPPARKS simulation. Solid black and blue lines indicate the fitted trendlines for the HEDM and SPPARKS data, respectively. R^2 values are provided for the shown trendlines. (B, C) Cumulative distribution plots of the dV/A data in (A) for GBs within specified ranges of curvature in the (B) HEDM scans and (C) SPPARKS simulations.

of shared voxel faces between grains at t_0. In the sign convention used here, positive dV/A indicates a boundary moving away from its center of curvature and negative dV/A is a boundary moving towards its center of curvature. GBs are expected to move towards their center of curvature (i.e., negative dV/A). The average mean curvature (κ) was calculated by

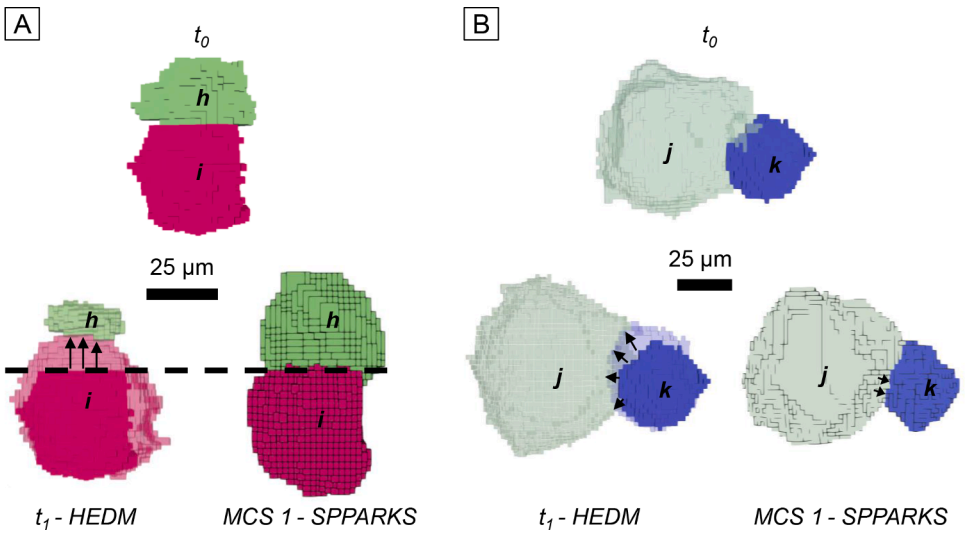

Fig. 4. Grains (A) h and i and (B) j and k before (t_0) and after (t_1) grain growth as observed by HEDM and in the SPPARKS simulation. Note that the microstructure at t_0 is the same for the HEDM and SPPARKS simulation and, thus, only shown once. (B) Example of flat GB (k = 0 μm^{-1}) that moves significantly in the experiment but is stationary in the simulation. The black dashed line indicates the GB position at t_0. (B) Example of curved GB that moves in the direction away from its center of curvature in the experiment but not in the simulation. The grains from t_1 HEDM scan are partially transparent to reveal the original position of the grains (shown as opaque voxels). Arrows indicate the direction of GB movement.

dividing each GB's M_s by its area. The curvatures were measured from the initial time step and, thus, identical for the HEDM and SPPARKS datasets. Only boundaries with greater than 100 voxel faces (400 μm^2) or associated with grains having diameters greater than 10 μm were included in this analysis (3329 GBs).

Fig. 3A shows the average and standard deviation of dV/A for the same GBs in the HEDM and SPPARKS datasets over specified ranges of κ (bin size of 0.002 μm^{-1}). The variation found in the HEDM data is significantly greater than the SPPARKS simulation. In the SPPARKS simulation, the negative linear trend with curvature is statistically validated ($R^2 = 0.91$), indicating that again the GBs move towards their center of curvature. In contrast, no clear evidence for a linear relationship can be extracted from a fit of dV/A to κ ($R^2 = 0.12$) for the experimental data.

To demonstrate that the HEDM data shows no statistical relationship between dV/A with κ, the distributions shown in Figs. 3B and 3C were compared with a Kolmogorov-Smirnov goodness-of-fit test. For the HEDM data, the null hypothesis that the dV/A distributions for each curvature range were different from one another could not be rejected (all calculated p-values greater than 0.04), indicating that curvature is not a good descriptor of a GB's motion. In contrast, the same hypothesis was rejected for the dV/A distributions in the isotropic simulation. For example, for the SPPARKS data, there is a probability of 8 $\times 10^{-13}$ that the distribution of dV/A values observed for GBs with curvatures between 0.00 and 0.002 μm^{-1} is from the same distribution as those with curvatures between 0.028 and 0.030 μm^{-1}. Therefore, GBs generally move according to curvature in the isotropic simulation.

Notably, larger magnitudes of dV/A are observed in the HEDM data set than in the SPPARKS data, despite the similar number of grains lost during growth. The average magnitude of dV/A is 1.9 ± 1.7 μm and 0.8 ± 0.6 μm for GBs in the HEDM and SPPARKS simulation, respectively. Additionally, there are many observations of unexpected GB motion in the HEDM data. The average dV/A for flat boundaries (k = 0 μm^{-1}) is 2.3 μm, which is greater than calculated for those same flat boundaries in the SPPARKS simulation (0.7 μm) and the curved boundaries. Fig. 4A shows a GB that is perfectly flat (κ = 0 μm^{-1}) that does not move during the simulation. However, HEDM observations show that Grain *i* grows at the expense of Grain *h*.

Significantly, 37% of the total GBs in the HEDM data are *migrating in the direction opposite of their center of curvature*, as seen for the boundaries with positive dV/A in Fig. 3. Furthermore, 30% of boundaries with κ greater than or equal to 0.02 μm^{-1} have positive dV/A. Fig. 4B shows an example of such *anti-curvature* motion: Grain *j* is expected to grow at the expense of Grain *k* due to the curvature of the shared GB at t_0, but the opposite is observed. In the simulation, the same GB reduces its area by flattening such that Grain *j* grows at the expense of Grain *k* (shown by the arrows). In the SPPARKS simulation, 22% of all GBs and only 8% of boundaries with κ greater than or equal to 0.02 μm^{-1} exhibit anti-curvature motion. These observations suggest that curvature alone is not driving the motion locally and that GBs find other pathways to minimize energy of the system.

To validate this unexpected behavior, potential errors associated with the dV/A and curvature measurements were investigated. As discussed in the supplementary information, error associated with misregistering the two volumes in 3D space was minimized such that it has no significant impact on the measured dV/A values. Imprecise curvature measurements using Eq. (1) may be responsible for some of the scatter in Fig. 3. The finding of GBs in the SPPARKS simulation moving against their curvature (i.e., GBs with positive dV/A), which is unexpected in simulations using isotropic GB energy, does suggest that Eq. (1) has some degree of uncertainty. However, the imprecision of the curvature measurements cannot account for why the migration *direction* for the same boundary differs between HEDM and simulation. Of the nonzero curvature GBs evaluated, again 37% of GBs in the HEDM measurements move in the opposite direction of the simulation. From these assessments, the unexpected behavior shown in Fig. 3A cannot be an artifact of the curvature or dV/A calculations.

GB anisotropy may account for the large variation in velocities observed in the HEDM data. In anisotropic systems, there is no single velocity function because mobility and energy are unique for different GB types. Therefore, certain GBs may be more sensitive to curvature than others in $SrTiO_3$, which is a system with prior evidence of both anisotropic energy [27] and mobility [28]. The observations here would suggest that the differences in mobility and energy between individual GBs may outweigh the curvature component during grain growth in a 3D system similar to the HEDM study of Ni [15]. Further evidence of the absence of a correlation between curvature and velocity is found in a grain growth study by Zhang et al. in iron [29]. In that work, reduced mobilities were computed based on the assumption that velocity was proportional to curvature and yielded values that were not constant with time for the same boundary nor with GB crystallography, drawing into question the assumed proportionality. Further work is necessary to explore how anti-curvature motion lowers the overall interfacial energy in an anisotropic GB network.

Here, we have demonstrated that HEDM studies provide critical observations of grain growth in real polycrystals. In particular, this HEDM study revealed the following unexpected aspects of grain growth in $SrTiO_3$:

1 Neither the number of neighbors nor the local curvature correlates with experimentally observed grain growth in $SrTiO_3$, as determined over a narrow range of grain growth.
2 Larger GB velocities are observed in the experimental data than in the SPPARKS simulation.
3 Experimentally, ~37% of measurable GBs move in the direction *opposite* to their center of curvature.

Further investigations exploring the properties of particular GB types are necessary to understand how the observed migration reduces the total GB energy. These findings support the need for 4D experimental grain growth studies to test our assumptions about grain growth.

Declaration of Competing Interest

The authors declare that they have no known competing financial interests or personal relationships that could have appeared to influence the work reported in this paper.

Acknowledgments

The authors would like to thank Dr. Michael J. Hoffmann for the $SrTiO_3$ samples. Additionally, they would like to thank Jun-Sang Park and Peter Kenesei for their assistance in data collection. This material is based upon work supported by the W.M. Keck Foundation and the National Science Foundation Graduate Research Fellowship Program under grant no. AWD04512-1842473. Dr. Rohrer also acknowledges support from the National Science Foundation under grant DMR 2118945. This research used resources of the Advanced Photon Source, a U.S. Department of Energy (DOE) Office of Science user facility operated for the DOE Office of Science by Argonne National Laboratory under contract no. DE-AC02-06CH11357. In addition, the authors are grateful to the Argonne National Laboratory for the allotment of beam time on beamline 1-ID-B,C,E at the Advanced Photon Source (Proposal 63745). The HEDM measurements were made possible by preliminary 3D characterizations of $SrTiO_3$ carried out at beamline BL20XU of the Japan Synchrotron Radiation Research Institute (SPring-8), Proposals 2017A1534 and 2018A1521.

Supplementary materials

Supplementary material associated with this article can be found, in the online version, at doi:10.1016/j.scriptamat.2022.115055.

References

[1] J.E. Burke, D. Turnbull, Progr. Metal Phys. 3 (1952) 220–292.
[2] R.J. BROOK, J. Am. Ceram. Soc. 52 (1969) 56–57, https://doi.org/10.1111/j.1151-2916.1969.tb12664.x.
[3] M. Hillert, Acta Metall. 13 (1965) 227–238, https://doi.org/10.1016/0001-6160(65)90200-2.
[4] J.W. Cahn, Acta Metall. 10 (1962) 789–798, https://doi.org/10.1016/0001-6160(62)90092-5.
[5] F.J. Humphreys, Acta Metall. 45 (1997) 4231–4240.
[6] M. Upmanyu, G.N. Hassold, A. Kazaryan, E.A. Holm, Y. Wang, B. Patton, D. J. Srolovitz, Interface Sci. 10 (2002) 201–216, https://doi.org/10.1023/A:1015832431826.
[7] D.J. Srolovitz, G.S. Grest, M.P. Anderson, Acta Metall. 33 (1985) 2233–2247, https://doi.org/10.1016/0001-6160(85)90185-3.
[8] D.A. Molodov, U. Czubayko, G. Gottstein, L.S. Shvindlerman, Scr. Metall. 32 (1995) 529–534.
[9] J.v. Bernier, R.M. Suter, A.D. Rollett, J.D. Almer, Annu. Rev. Mater. Res. 50 (2020) 395–436, https://doi.org/10.1146/annurev-matsci-070616-124125.
[10] W. Ludwig, S. Schmidt, E.M. Lauridsen, H.F. Poulsen, J. Appl. Crystallogr. 41 (2008) 302–309.
[11] U. Lienert, S.F. Li, C.M. Hefferan, J. Lind, R.M. Suter, J.v. Bernier, N.R. Barton, M. C. Brandes, M.J. Mills, M.P. Miller, B. Jakobsen, W. Pantleon, JOM 63 (2011) 70–77, https://doi.org/10.1007/s11837-011-0116-0.
[12] S. Schmidt, S.F. Nielsen, C. Gundlach, L. Margulies, X. Huang, D.J. Jensen, Science (1979) 305 (2004) 229–232, https://doi.org/10.1126/science.1098627.
[13] S.A. McDonald, P. Reischig, C. Holzner, E.M. Lauridsen, P.J. Withers, A.P. Merkle, M. Feser, Sci. Rep. 5 (2015) 14665.
[14] B.R. Patterson, R.T. Dehoff, C.A. Sahi, J. Sun, J. Oddershede, F. Bachmann, E. Lauridsen, D.J. Jensen, IOP Conf. Ser. Mater. Sci. Eng. 580 (2019), https://doi.org/10.1088/1757-899X/580/1/012020.
[15] A. Bhattacharya, Y.F. Shen, C.M. Hefferan, S.F. Li, J. Lind, R.M. Suter, C.E. Krill, G. S. Rohrer, Science (1979) 374 (2021) 189–193, https://doi.org/10.1126/science.abj3210.
[16] M. Bäurer, H. Kungl, M. Hoffmann, J. Am. Ceram. Soc. 606 (2009) 601–606, https://doi.org/10.1111/j.1551-2916.2008.02920.x.
[17] Y. Zhu, P.A. Salvador, G.S. Rohrer, Phys. Chem. Chem. Phys. 19 (2017) 7910–7918, https://doi.org/10.1039/c6cp08608j.
[18] H. Liu, R.M. Suter, HEXOMAP (2021). https://github.com/HeLiuCMU/HEXOMAP.
[19] A. M. Groeber, M. Jackson, A. Integr. Mater. Manuf. Innov. 3 (2014) 5, https://doi.org/10.1186/2193-9772-3-5.
[20] C.Garcia Cardona, G. Wagner, V. Tikare, E. Holm, S. Plimpton, A. Thompson, A. Slepoy, X. Zhou, C. Battaile, M. Chandross, Crossing the mesoscale no-man's land via parallel kinetic Monte Carlo., Albuquerque, NM, and Livermore, CA (United States), 2009. https://doi.org/10.2172/966942.
[21] D. Zöllner, Comput. Mater. Sci. 86 (2014) 99–107, https://doi.org/10.1016/j.commatsci.2014.01.044.
[22] D. Zöllner, Comput. Mater. Sci. 50 (2011) 2712–2719, https://doi.org/10.1016/j.commatsci.2011.04.024.
[23] J. von Neumann, Shape of Metal Grains. Metal Interfaces, ASM, Cleveland, OH, 1952, p. 108.
[24] W.W. Mullins, J. Appl. Phys. 27 (1956) 900–904, https://doi.org/10.1063/1.1722511.
[25] X. Zhong, M.N. Kelly, H.M. Miller, S.J. Dillon, G.S. Rohrer, J. Am. Ceram. Soc. 102 (2019) 7003–7014, https://doi.org/10.1111/jace.16608.
[26] D.J. Rowenhorst, A.C. Lewis, G. Spanos, Acta Mater. 58 (2010) 5511–5519, https://doi.org/10.1016/j.actamat.2010.06.030.
[27] W. Rheinheimer, M. Bäurer, H. Chien, G.S. Rohrer, C.A. Handwerker, J.E. Blendell, M.J. Hoffmann, Acta Mater. 82 (2015) 32–40, https://doi.org/10.1016/j.actamat.2014.08.065.
[28] W. Rheinheimer, M. Bäurer, C.A. Handwerker, J.E. Blendell, M.J. Hoffmann, Acta Mater. 95 (2015) 111–123, https://doi.org/10.1016/j.actamat.2015.05.019.
[29] J. Zhang, W. Ludwig, Y. Zhang, H.H.B. Sørensen, D.J. Rowenhorst, A. Yamanaka, P. W. Voorhees, H.F. Poulsen, Acta Mater. 191 (2020) 211–220, https://doi.org/10.1016/j.actamat.2020.03.044.